Prediction of mechanical solutions for a laminated LCEs system fusing an analytical model and neural networks

Wang, Jue ; Yuan, Weiyi; Li, Zichuan; Zhu, Yingcan ; Santos, Thebano ; Fan, Jiajie

DOI
10.1016/j.jmbbm.2021.104918

Publication date
2022

Document Version
Final published version

Published in
Journal of the Mechanical Behavior of Biomedical Materials

journal of the mechanical behavior of biomedical materials 125 (2022) 104918

Contents lists available at ScienceDirect

Journal of the Mechanical Behavior of Biomedical Materials

journal homepage: www.elsevier.com/locate/jmbbm

Research Paper

Prediction of mechanical solutions for a laminated LCEs system fusing an analytical model and neural networks

Jue Wang [a], Weiyi Yuan [a], Zichuan Li [c], Yingcan Zhu [d], Thebano Santos [e], Jiajie Fan [b,c,*]

[a] College of Mechanical & Electrical Engineering, Hohai University, Changzhou, 213022, China
[b] Institute of Future Lighting, Academy for Engineering & Technology, Fudan University, Shanghai, 200433, China
[c] Department of Microelectronics, Delft University of Technology, 2628, CD, Delft, the Netherlands
[d] Centre for Sustainable Agricultural Systems, University of Southern Queensland, West St, Toowoomba, Queensland 4350, Australia
[e] Center of Information Technology "Renato Archer" (CTI), Ministry of Science, Technology, Innovation and Communication, Brazil

ARTICLE INFO

Keywords:
Laminated liquid crystal elastomers system
Thermo-mechanical load
Analytical solution
BP neural Network

ABSTRACT

This paper presents a convenient and efficient method to predict the mechanical solutions of a laminated Liquid Crystal Elastomers (LCEs) system subjected to combined thermo-mechanical load, based on a back propagation (BP) neural network which is trained by machine learning from a database established by analytical solutions. Firstly, the general solutions of temperature, displacement, and stress of any single layer in the LCEs system are obtained by solving the two-dimensional (2D) governing equations of both heat conduction and thermoelasticity. Then, the unknown coefficients in above general solutions are determined by a transfer-matrix method based on the continuity condition at the interface of adjacent layers and the combined thermo-mechanical loads condition at the surface of the LCEs system. The formula derivation and calculator program are verified through convergence studies and comparisons with FEM results. Finally, a database with displacements of LCEs system in a temperature field subjected to 561 sets of mechanical loads is established based on the presented analytical model. The BP neural network based on above database is further applied to establish the relationship between deformation and mechanical load to predict the elastic deformation of the LCEs system in a temperature field subjected to a mechanical load. Moreover, the BP network can also inverse the coefficients of mechanical load which induces the specific deformation in a temperature field. The numerical examples show that: (1) The deformation of a laminated LCEs system due to thermal load is limited within the range of human temperature changes from 36 °C to 40 °C. (2) The thickness of the LCE is a sensitive parameter on the deformation at the bottom surface of the system. (3) The accuracy of predicted displacements induced by the thermo-mechanical load and the inversed mechanical load based on deformation of the LCEs system in a temperature field using BP neural network reaches 99.6% and 98.5% respectively.

1. Introduction

Heart failure and stroke associated with atrial fibrillation are the most terrible and common diseases. Mechanical atrial contractile assist devices can effectively reduce the mortality and incidence rate of patients. Therefore, using intelligent materials to support atrial contractile function is put forward. Liquid Crystal Elastomer is one of smart biomedical materials which is usually called artificial muscles, since it can respond reversibly to external stimulation such as temperature and result in unique movement or tension (Gennes et al., 1997). Many researches (Thomsen et al., 2001; Li et al., 2004) show that LCEs will become contraction with the increase of temperature. It means that LCEs have negative thermal expansion. P. D. Gennes (1997) found that through the change of temperature, the LCE is stimulated to produce deformation, which is very similar to the work of human muscles. However, LCEs system is generally laminated with other material layers to meet some special functional requirements in architecture (Lu et al., 2019; Shenoy et al., 2002). Therefore, it's a trend to develop new generation of cardiac systolic assist device consisting of laminated LCEs with flexible substrate material and attached to the surface of the heart to support atrial contractile function. For such atrial contractile assist devices, the relationship between a continuously distributed mechanical load and the deformation at the bottom surface of a laminated LCEs system in a temperature field is a significant mechanical performance

* Corresponding author. Institute of Future Lighting, Academy for Engineering & Technology, Fudan University, Shanghai, 200433, China.
E-mail address: jiajie_fan@fudan.edu.cn (J. Fan).

https://doi.org/10.1016/j.jmbbm.2021.104918
Received 20 July 2021; Received in revised form 9 October 2021; Accepted 19 October 2021
Available online 29 October 2021

worth paying attention to.

The LCEs system can be modelled as a simply supported laminated beam subjected to combined thermo-mechanical load. Many researchers have made great efforts in the analysis of laminated beams based on various theories, such as the classical beam theory (CBT) (Sharma and Kaur, 2015), first-order shear deformation theory (FOSDT) (Asadi et al., 2014) and higher-order shear deformation theory (HOSDT) (Thai and Vo, 2012; Wu and Zhao, 2012). The CBT based on Euler-Bernoulli hypothesis is popular in engineering due to its simplicity. As the influence of transverse shear deformation is ignored, the calculation accuracy of thick beam in the classical theory is low (Ren et al., 2021). FOSDT is proposed by assuming the through-thickness distribution of transverse shear strain to be constant and hence has been widely applied into thermo-mechanical problems. Timoshenko (1925) pioneered FOSDT to solved the bending of bi-metal strip under uniform thermal loads. However, the assumed constant transverse shear strain component is considered with their respectively shear correction factor. This value depends on the material coefficients, geometry, boundary conditions and loading conditions, which is difficult to calculate. Therefore, HOSDT is further introduced to avoid the shear correction factors. It is developed based on the assumption of a higher-order variation of axial and transverse displacements through the depth of the beam. Kapuria et al. (2003) used a new high-order zigzag line theory to analyse the thermal stress of composite beams under thermal load. In addition, Carrera Unified Formulation (CUF) is a more beneficial alternative in the analysis of laminated beams, plates, and shells (Carrera and Giunta, 2010; Carrera, 2001; Carrera et al., 2016a). CUF considers the transverse deflection as a function with Taylor's expansions of *N*-order, which is a major advantage because the effect of transverse normal strain can be considered in the analysis. Carrera and his collaborators (Giunta et al., 2013; Carrera et al., 2016b) have successfully proposed a class of the 1D finite element-CUF models for static uncoupled thermoelastic analysis of some complex structures with non-uniform cross-section. This method has the advantages of high precision in the bending frequency computation, high reliability in predicting complex phenomena, and significant capability in reducing the computational cost.

Comparing with the results based on CBT, FOSDT, and HOSDT, the results based on the elasticity theory are more accurate since no hypotheses introduced in the analysis (Eslami et al., 2013; Xu and Zhou, 2009, 2012). The analytical solution based on the elasticity theory not only ensures the calculation accuracy, but also has a higher calculation efficiency than finite element numerical method. Eslami et al. (2013) reviewed the thermoelastic theory and presented its application in some practical problem. Xu et al. (Xu and Zhou, 2009, 2012) studied the thermoelastic solutions of simply supported beams and plates with variable thickness under mechanical and thermal loads. The above researches used the thermoelastic theory to present the analytical solution of a single-layer structure and laid theoretical foundation for the analysis of multi-layer laminated structures. Blanc M et al. (Blanc and Touratier, 2007) proposed an analytical model of heat conduction for multi-layer structures based on the equivalent single-layer method, which can satisfy both the continuity of temperature and normal heat flux at the interface. Qian et al., 2015a, 2015b presented the analytical solutions of temperature, displacement and stress of simply supported composite beams and plates under thermal load based on the 2D thermoelastic theory. Based on the similar 2D thermoelastic theory, Zhang et al. (2019) analysed the influence of temperature field on the mechanical properties of a laminated beam made of temperature-dependent materials.

It should be noted that above researches presented different methods to obtain the mechanical solutions of laminated beams subjecting to different loads. However, it is of practical significance to present a simple calculation scheme that can establish the relationship between the deformation and the load of the multi-layer laminated beams. And then, engineers can get rid of the original cumbersome calculation and predict the mechanical solutions of a laminated system more conveniently and quickly. As a method of machine learning, the Artificial Neural Network (ANN) is a mathematical computing system inspired by the biological neural network in which try to constitute human brain for learning and analysis to achieve self-optimization (Mitchell, 2003). It can be used to classify, predict, and cluster data. ANN can acquire, represent, and compute a mapping from one multivariate space of information to another. Back propagation neural network is one of the most common applications of ANN to predict the certain outputs based on the training of input parameters (Hagan et al., 2002). The ANN prediction method is successfully applied to various fields of engineering (Mitchell, 2003; Hagan et al., 2002; Balla et al., 2021; Do et al., 2020; Bagheripoor and Bisadi, 2013; Sattari et al., 2013). Pidaparti and Palakal (2015) developed a BP neural network to predicting the stress-strain behaviour of graphite-epoxy laminates based on a training experimental data set consisting of 959 points. Teti et al. (Teti and Caprino, 1994) used an artificial neural network to accurately predict the residual tensile strength of composite laminates containing artificially implanted holes based on the experimental results. Ziane et al. (2015) used an artificial neural network to accurately predict the fatigue strength of composite laminates with different fiber orientations. The above researches indicate that ANN have been used in modelling the mechanical behaviour of composite materials. However, few studies have applied neural network to the study and prediction of mechanical properties of laminated beams subjected to combined thermo-mechanical loads.

In this paper, a mechanical atrial contractile assist devices made of layered liquid crystal elastomer is modelled as a simply supported laminated beams. An analytical solution based on two-dimensional thermoelastic theory of simply supported laminated LCEs system subjected to thermo-mechanical loads is presented in this paper to establish a database that used to train BP neural network models for the prediction of mechanical solutions. The convergence studies and comparisons with FEM results are presented to confirm the validity of the formula derivation and calculator program of the analytical solution. Some parametric studies are presented by using analytical model to analyse the influence of the thermo-mechanical loads, and the thickness of LCE on the mechanical properties of the LCEs system. The BP artificial neural network established from learning the above database is further applied to predict the elastic deformation which induced by mechanical load in the specific temperature field. Moreover, the BP method based on the database can also inverse the coefficients of mechanical load which induces the deformation of the LCEs system in the specific temperature field. The mechanical solutions of a laminated LCEs system obtained from the trained BP neural network models are also compared with original results to evaluate the predicting accuracy.

2. Theoretical model

2.1. Analytical model for a simply supported multi-layered LCEs system

2.1.1. Basic equations and general solutions of the i-th layer in system

A laminated LCEs system with length L and thickness H is simplified as a simply supported two-dimensional beam model with p layers as shown in Fig. 1(a). Since the LCEs system in human body may subject to a fever, the temperature within the beam increases and reaches stability. Finally, the temperatures on the top and bottom surfaces of the beam are stable at T_t (x) and T_b (x) along the beam. Meanwhile, the bottom surface of the beam is subjected to a continuously distributed mechanical load $q(x)$. To conveniently analyse the mechanical performance of the i-th layer ($i = 1, 2, \ldots p$) with uniform thickness h_i of the beam, a local Cartesian coordinate system as shown in Fig. 1(b) is built with the axes along the length and thickness denoted by x and y_i, respectively. The material properties of the i-th layer are described by the elastic modulus E_i, the Poisson ratio μ_i, the thermal expansion coefficient α_i and the thermal conductivity k_i.

Consider an arbitrary i-th layer in the local Cartesian coordinate

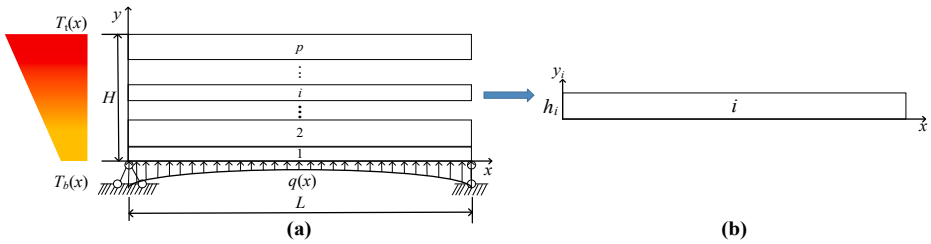

Fig. 1. Two-dimensional multi-layer simply supported beam under combined thermo-mechanical load.

system x-y_i, the 2D heat conduction equation is given as

$$\frac{\partial^2 T_i(x,y_i)}{\partial x^2}+\frac{\partial^2 T_i(x,y_i)}{\partial y_i^2}=0 \tag{1}$$

Where T_i (x,y_i) is the temperature distribution field of the i-th layer.

The general solution of Eq. (1) can be approximately expanded in Fourier series with finite terms as

$$T_i(x,y_i)=\sum_{m=1}^{\infty} t_{mi}(y_i)\sin(\alpha_m x) \tag{2}$$

Where $\alpha_m = m\pi/L$. Combined with Eq. (2) and Eq. (1), T_i (x,y_i) can be expressed as

$$T_i(x,y_i)=\sum_{m=1}^{\infty}[E_{mi}\cosh(\alpha_m y_i)+F_{mi}\sinh(\alpha_m y_i)]\sin(\alpha_m x) \tag{3}$$

E_{mi} and F_{mi} are unknown coefficients depending on the temperature conditions at the upper and lower surfaces of the i-th layer.

The two-dimensional thermoelastic constitutive equations for the i-th beam layer are given as

$$\begin{aligned}
\sigma_{xi}(x,y_i)&=\frac{E_i}{1-\mu_i^2}\left(\frac{\partial u_i(x,y_i)}{\partial x}+\mu_i\frac{\partial v_i(x,y_i)}{\partial y_i}\right)-\frac{E_i\alpha_i T_i(x,y_i)}{1-\mu_i},\\
\sigma_{yi}(x,y_i)&=\frac{E_i}{1-\mu_i^2}\left(\frac{\partial v_i(x,y_i)}{\partial y_i}+\mu_i\frac{\partial u_i(x,y_i)}{\partial x}\right)-\frac{E_i\alpha_i T_i(x,y_i)}{1-\mu_i},\\
\tau_{xyi}(x,y_i)&=\frac{E_i}{2(1+\mu_i)}\left(\frac{\partial v_i(x,y_i)}{\partial x}+\frac{\partial u_i(x,y_i)}{\partial y_i}\right)
\end{aligned} \tag{4}$$

Where $\sigma_{xi}(x,y_i)$ and $\sigma_{yi}(x,y_i)$ are the normal stresses of the i-th layer respectively; $\tau_{xyi}(x,y_i)$ is the shear stress. $u_i(x,y_i)$ and $v_i(x,y_i)$ are the displacements in the x and y directions respectively. In the absence of body forces, the stress components of the i-th layer should satisfy the following equilibrium equations

$$\frac{\partial\sigma_{xi}(x,y_i)}{\partial x}+\frac{\partial\tau_{xyi}(x,y_i)}{\partial y_i}=0,\frac{\partial\sigma_{yi}(x,y_i)}{\partial y_i}+\frac{\partial\tau_{xyi}(x,y_i)}{\partial x}=0 \tag{5}$$

To satisfy the following boundary condition of a simply supported beam

$$\sigma_{xi}(0,y_i)=\sigma_{xi}(L,y_i)=0,v_i(0,y_i)=v_i(L,y_i)=0 \tag{6}$$

the general solutions of displacement fields for the i-th layer can be assumed as

$$u_i(x,y_i)=\sum_{m=1}^{\infty}U_{mi}(y_i)\cos(\alpha_m x),v_i(x,y_i)=\sum_{m=1}^{\infty}V_{mi}(y_i)\sin(\alpha_m x) \tag{7}$$

By substituting Eq. (7) into Eqs. (4) and (5), two differential equations concerning $U_{mi}(y_i)$ and $V_{mi}(y_i)$ can be derived. Then, the displacement fields and stress fields of the i-th layer can be figured out and rewritten in a matrix form as follows

$$\begin{bmatrix} u_i(x,y_i)\\ v_i(x,y_i)\\ \sigma_{xi}(x,y_i)\\ \sigma_{yi}(x,y_i)\\ \tau_{xyi}(x,y_i)\end{bmatrix}=\sum_{m=1}^{\infty}\left\{\begin{bmatrix} TF_{mi}^{11} & TF_{mi}^{12} & TF_{mi}^{13} & TF_{mi}^{14}\\ TF_{mi}^{21} & TF_{mi}^{22} & TF_{mi}^{23} & TF_{mi}^{24}\\ TF_{mi}^{31} & TF_{mi}^{32} & TF_{mi}^{33} & TF_{mi}^{34}\\ TF_{mi}^{41} & TF_{mi}^{42} & TF_{mi}^{43} & TF_{mi}^{44}\\ TF_{mi}^{51} & TF_{mi}^{52} & TF_{mi}^{53} & TF_{mi}^{54}\end{bmatrix}\begin{bmatrix} A_{mi}\\ B_{mi}\\ C_{mi}\\ D_{mi}\end{bmatrix}+\begin{bmatrix} TT_{mi}^{11} & TT_{mi}^{12}\\ TT_{mi}^{21} & TT_{mi}^{22}\\ TT_{mi}^{31} & TT_{mi}^{32}\\ TT_{mi}^{41} & TT_{mi}^{42}\\ TT_{mi}^{51} & TT_{mi}^{52}\end{bmatrix}\begin{bmatrix} E_{mi}\\ F_{mi}\end{bmatrix}\right\}\times\begin{bmatrix}\cos(\alpha_m x)\\ \sin(\alpha_m x)\\ \sin(\alpha_m x)\\ \sin(\alpha_m x)\\ \cos(\alpha_m x)\end{bmatrix} \tag{8}$$

The unknown coefficients A_{mi}, B_{mi}, C_{mi} and D_{mi} in the general solutions of Eq. (8) will be obtained based on the two following boundary conditions. Firstly, the continuity of displacements and stresses between adjacent layers of laminated beams. Secondly, the force boundary conditions at the top and bottom surfaces of the beam. Similarly, the unknown coefficients E_{mi} and F_{mi} will be obtained based on the temperature continuity of adjacent layers and the temperature boundary condition at the top and bottom surfaces of the laminated beam. The expressions of the elements in matrix $\boldsymbol{TF}_{mi}$ and matrix $\boldsymbol{TT}_{mi}$ are shown in Appendix.

2.1.2. Determine the coefficients of temperature field

According to Eq. (2), the temperature and heat flux in the beam can be expressed as:

$$\begin{bmatrix} T_i(x,y_i)\\ k_i\dfrac{\partial T_i(x,y_i)}{\partial y_i}\end{bmatrix}=\sum_{m=1}^{\infty}\boldsymbol{K}_{mi}(y_i)\sin(\alpha_m x) \tag{9}$$

From Eq. (3), $\boldsymbol{K}_{mi}(y_i)$ can be expressed as:

$$\boldsymbol{K}_{mi}(y_i)=\boldsymbol{C}_{mi}(y_i)\begin{bmatrix} E_{mi} & F_{mi}\end{bmatrix}^T \tag{10}$$

in which $\boldsymbol{C}_{mi}(y_i)=\begin{bmatrix}\cosh(\alpha_m y_i) & \sinh(\alpha_m y_i)\\ k_i\alpha_m\sinh(\alpha_m y_i) & k_i\alpha_m\cosh(\alpha_m y_i)\end{bmatrix}$.

Then, the relationship of the temperature and heat flux on the upper and lower surfaces of the i-th layer can be deduced from Eq. (10) as $\boldsymbol{K}_{mi}(h_i)=[\boldsymbol{C}_{mi}(h_i)\boldsymbol{C}_{mi}^{-1}(0)]\boldsymbol{K}_{mi}(0)$. Following the continuity of temperature and heat flux between the upper surface of the i-th layer and the lower surface of the i+1-th layer of the laminated beam, i. e. $\boldsymbol{K}_{m(i+1)}(0)=\boldsymbol{K}_{mi}(h_i)$, the relationship between the temperature and heat flux of the

q-th layer ($q = 1,2, \ldots p$) and the first layer can be obtained:

$$[E_{mq} \quad F_{mq}]^T = \left\{ \boldsymbol{C}_{mq}^{-1}(h_q) \left[\prod_{i=q}^{1} \boldsymbol{C}_{mi}(h_i) \boldsymbol{C}_{mi}^{-1}(0) \right] \right\} \boldsymbol{C}_{m1}(0) [E_{m1} \quad F_{m1}]^T \tag{11}$$

The temperature boundary condition of the top and bottom surfaces of the laminated beam is:

$$T_1(x,0) = T_b(x), T_p(x,h_p) = T_t(x) \tag{12}$$

Substituting Eq. (3) into Eq. (12) and using Fourier series, Eq. (12) can be expressed in the following form:

$$\begin{cases} E_{m1} = \dfrac{2}{L} \displaystyle\int_0^L T_b(x) \sin(\alpha_m x) dx \\ \cosh(\alpha_m h_p) E_{mp} + \sinh(\alpha_m h_p) F_{mp} = \dfrac{2}{L} \displaystyle\int_0^L T_t(x) \sin(\alpha_m x) dx \end{cases} \tag{13}$$

$$\boldsymbol{W}_{mi}(h_i) = \boldsymbol{D}_{mi}(h_i) \boldsymbol{D}_{mi}^{-1}(0) [\boldsymbol{W}_{mi}(0) - \boldsymbol{G}_{mi}(0)] + \boldsymbol{G}_{mi}(h_i) \tag{16}$$

Considering the continuity of displacements and stresses between adjacent layers of laminated beams, the displacement and stress on the upper surface of the i-th layer beam must be equal to these on the lower surface of the (i+1)-th layer, i.e. $\boldsymbol{W}_{m(i+1)}(0) = \boldsymbol{W}_{mi}(h_i)$. Based on the transfer matrix method, the relationships of the displacement and stress between the upper surface of the q-th layer ($q = 1,2, \ldots p$) and the lower surface of the first layer can be obtained as:

$$\boldsymbol{W}_{mq}(h_q) = \begin{bmatrix} U_m^{11} & U_m^{12} \\ U_m^{21} & U_m^{22} \end{bmatrix} \boldsymbol{W}_{m1}(0) + [S_m^1 \quad S_m^2 \quad S_m^3 \quad S_m^4]^T \tag{17}$$

Where $\begin{bmatrix} U_m^{11} & U_m^{12} \\ U_m^{21} & U_m^{22} \end{bmatrix} = \prod_{i=q}^{1} \boldsymbol{D}_{mi}(h_i) \boldsymbol{D}_{mi}^{-1}(0)$

$$[S_m^1 \quad S_m^2 \quad S_m^3 \quad S_m^4]^T = -\sum_{j=1}^{q} \left\{ \prod_{i=q}^{j} [\boldsymbol{D}_{mi}(h_i) \boldsymbol{D}_{mi}^{-1}(0)] \right\} \boldsymbol{G}_{mj}(0) + \sum_{j=2}^{q} \left\{ \prod_{i=q}^{j} [\boldsymbol{D}_{mi}(h_i) \boldsymbol{D}_{mi}^{-1}(0)] \right\} \boldsymbol{G}_{m(j-1)}(h_{j-1}) + \boldsymbol{G}_{mq}(h_q)$$

Combined with Eq. (11) and Eq. (13) in the case of $q = p$, E_{m1}, F_{m1}, E_{mp} and F_{mp} can be solved. Then submitting E_{m1}, F_{m1} into Eq. (11), the unknown coefficients E_{mi} and F_{mi} in arbitrary layer can be obtained. Finally, the temperature distribution field is obtained by substituting these coefficients E_{mi} and F_{mi} back into Eq. (3).

2.1.3. Determine the coefficients of displacement and stress fields

Eq. (8) can be rewritten as:

$$\begin{bmatrix} u_i(x,y_i) \\ v_i(x,y_i) \\ \sigma_{yi}(x,y_i) \\ \tau_{xyi}(x,y_i) \end{bmatrix} = \sum_{m=1}^{\infty} \boldsymbol{W}_{mi}(y_i) \times \begin{bmatrix} \cos(\alpha_m x) \\ \sin(\alpha_m x) \\ \sin(\alpha_m x) \\ \cos(\alpha_m x) \end{bmatrix} \tag{14}$$

Where

$$\boldsymbol{W}_{mi}(y_i) = \begin{bmatrix} U_{mi}(y_i) \\ V_{mi}(y_i) \\ Y_{mi}(y_i) \\ Z_{mi}(y_i) \end{bmatrix} = \boldsymbol{D}_{mi}(y_i) \begin{bmatrix} A_{mi} \\ B_{mi} \\ C_{mi} \\ D_{mi} \end{bmatrix} + \boldsymbol{G}_{mi}(y_i) \tag{15}$$

in which $\boldsymbol{D}_{mi}(y_i) = \begin{bmatrix} TF_{mi}^{11} & TF_{mi}^{12} & TF_{mi}^{13} & TF_{mi}^{14} \\ TF_{mi}^{21} & TF_{mi}^{22} & TF_{mi}^{23} & TF_{mi}^{24} \\ TF_{mi}^{41} & TF_{mi}^{42} & TF_{mi}^{43} & TF_{mi}^{44} \\ TF_{mi}^{51} & TF_{mi}^{52} & TF_{mi}^{53} & TF_{mi}^{54} \end{bmatrix}$, $\boldsymbol{G}_{mi}(y_i) = \begin{bmatrix} TT_{mi}^{11} & TT_{mi}^{12} \\ TT_{mi}^{21} & TT_{mi}^{22} \\ TT_{mi}^{41} & TT_{mi}^{42} \\ TT_{mi}^{51} & TT_{mi}^{52} \end{bmatrix} \begin{bmatrix} E_{mi} \\ F_{mi} \end{bmatrix}$.

It should be noticed that $\boldsymbol{G}_{mi}(y_i)$ here is a known functional matrix since the coefficients E_{mi}, F_{mi} have be obtained in section 2.1.2. According to Eq. (15), the relationship between the displacements and stresses of the upper and lower surfaces of the i-th layer has

A mechanical load is applied to the bottom surface of the laminated beam, and the boundary conditions of the top and bottom surfaces of the beam are

$$\sigma_{y1}(x,0) = q(x), \tau_{xy1}(x,0) = 0, \sigma_{yp}(x,h_p) = 0, \tau_{xyp}(x,h_p) = 0 \tag{18}$$

Using Fourier series, the mechanical load $q(x)$ can be expressed in the following form:

$$q(x) = \sum_{m=1}^{\infty} q_m \sin(\alpha_m x) \tag{19}$$

with $q_m = \frac{2}{L} \displaystyle\int_0^L q(x) \sin(\alpha_m x) dx$.

Substituting Eqs. (18) and (19) into Eq. (17), Eq. (17) can be divided into 2 s-order matrix equations as follows:

$$\begin{bmatrix} 0 \\ 0 \end{bmatrix} = U_m^{21} \begin{bmatrix} U_{m1}(0) \\ V_{m1}(0) \end{bmatrix} + U_m^{22} \begin{bmatrix} \dfrac{2}{L} \displaystyle\int_0^L q(x) \sin(\alpha_m x) dx \\ 0 \end{bmatrix} + \begin{bmatrix} S_m^3 \\ S_m^4 \end{bmatrix} \tag{20}$$

$$\begin{bmatrix} U_{mp}(h_p) \\ V_{mp}(h_p) \end{bmatrix} = U_m^{11} \begin{bmatrix} U_{m1}(0) \\ V_{m1}(0) \end{bmatrix} + U_m^{22} \begin{bmatrix} \dfrac{2}{L} \displaystyle\int_0^L q(x) \sin(\alpha_m x) dx \\ 0 \end{bmatrix} + \begin{bmatrix} S_m^1 \\ S_m^2 \end{bmatrix} \tag{21}$$

$U_{m1}(0)$ and $V_{m1}(0)$ can be obtained from the above equations. Then the unknown coefficients A_{mi}, B_{mi}, C_{mi} and D_{mi} can be further obtained by submitting $U_{m1}(0)$ and $V_{m1}(0)$ into the following equation which is combined by Eqs. (17) and (15):

$$\begin{bmatrix} A_{mi} \\ B_{mi} \\ C_{mi} \\ D_{mi} \end{bmatrix} = D_{mi}^{-1}(h_i)\left\{ \begin{bmatrix} U_m^{11} & U_m^{12} \\ U_m^{21} & U_m^{22} \end{bmatrix} \begin{bmatrix} U_{m1}(0) \\ V_{m1}(0) \\ \frac{2}{L}\int_0^L q(x)\sin(\alpha_m x)dx \\ 0 \end{bmatrix} + \begin{bmatrix} S_m^1 \\ S_m^2 \\ S_m^3 \\ S_m^4 \end{bmatrix} - G_{mi}(h_i) \right\} \tag{22}$$

Finally, substituting the coefficients back into Eq. (8), any unknown displacements and stresses of the system can be solved.

2.2. BP neural network prediction methods

The relationship between the deformation and the surface mechanical load at the bottom surface of LCEs system in a temperature field is a significant mechanical performance for the evaluation of an atrial contractile assist devices. The above presented analytical model provides an efficient method to calculate the deformation of the LCEs system in the case of a given combined thermo-mechanical load. However, the surface mechanical load cannot be inversed by a specific deformation in a temperature field according to the above analytical method. The artificial neural network, which is composed of several nodes connected to form an operation model, can imitate the human brain to handle a lot of disperse and parallel distributed data. Artificial neural network can obtain an unknown relationship between input and output information through training and learning of the database, and then complete the output of predicted data through the given input. The larger the database, the more accurate the output result. On the basis of this fact, a back propagation (BP) neural network (Liu et al., 2021) is introduced and applied to establish the relationship between deformation and mechanical load of the LCEs system in a temperature field.

BP neural network is a kind of artificial adaptive neural network with a multi-layer learning network structure and a way of supervised learning called back propagation algorithm. BP neural network belongs to static neural network with forward feedback. The output from BP networks only depends on the current input. The back propagation algorithm can minimize the mean square error between the predicted results and the expected ones by adjusting the weights. The prediction process using BP neural network is as follows: Firstly, the input information is propagated forward through the hidden layer to generate the output information. If there is an error between the output results and the expected results, the error will be propagated back. The error can be reduced by adjusting the weight and threshold based on the reverse information. After repeated learning and training, the weight and threshold corresponding to the minimum error are determined. Finally, the obtained weights are used to perform the output prediction of the new input data set.

A following polynomial function is presented to describe a continuously distributed symmetric mechanical load applied on the bottom surface of the LCEs system to establish the training database. With the increase of expansion order n, the function $q(x)$ can simulate different continuously distributed symmetric mechanical loads.

$$q(x) = \sum_{n=1}^{\infty} a_n (x - L/2)^{2n-2} \tag{23}$$

Where a_n ($n = 1, 2, 3, \ldots$) are the coefficients of the surface mechanical load. So the database used for training the BP artificial neural network can be established by selecting different expansion order n and different coefficients a_n of $q(x)$ to calculate the displacements of several points at the bottom surface of the laminated LCEs system in a temperature field based on the present analytical model.

As a machine learning method, the BP neural network consists of an input layer, a hidden layer and an output layer as shown in Fig. 2. The following equation is used to determine the number of hidden layers of the neural network.

$$N = \sqrt{O + I} + J \tag{24}$$

Where N, O and I are the number of hidden layers, output layers and input layers respectively. J is a constant in the range of 1 to 10 for

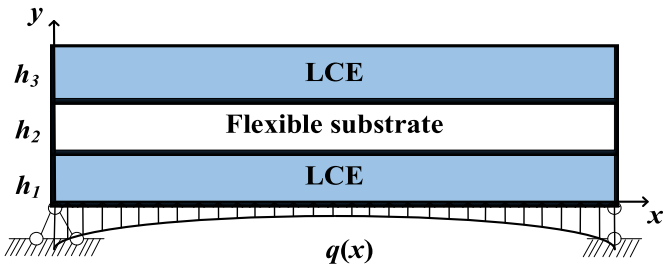

Fig. 3. The triple-layer LCEs system under combined thermo-mechanical load.

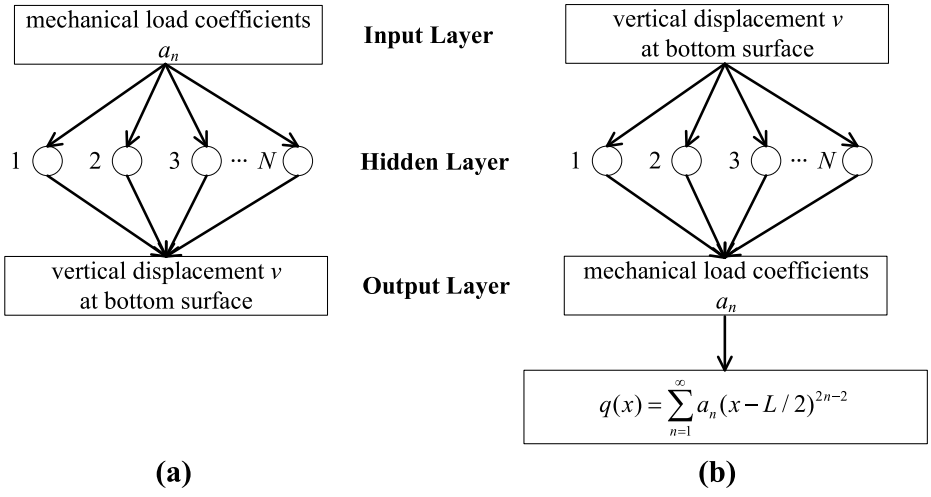

Fig. 2. The structure of the BP neural network: (a) predict the deformation based on the mechanical load; (b) inverse the mechanical load based on the deformation.

Table 1
Convergence of displacements under different mechanical loads in a temperature field.

$q(x)$ (N/cm)	Load graph	Position	Dis.	Expansion order m in the solution							
				5	10	15	20	25	30	35	40
0.1	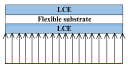	$x = 0.5$ cm,	u (μm)	−3.99	−4.16	−4.11	−4.11	−4.12	−4.11	−4.11	−4.11
		$y = 10$ μm	v (mm)	0.464	0.464	0.464	0.464	0.464	0.464	0.464	0.464
		$x = 1.5$ cm,	u (μm)	4.70	4.87	4.82	4.82	4.83	4.82	4.82	4.82
		$y = 20$ μm	v (mm)	0.464	0.464	0.464	0.464	0.464	0.464	0.464	0.464
$(x\text{-}1)^2$+0.1	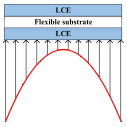	$x = 0.5$ cm,	u (μm)	−3.40	−3.57	−3.52	−3.52	−3.53	−3.52	−3.52	−3.52
		$y = 10$ μm	v (mm)	1.29	1.29	1.29	1.29	1.29	1.29	1.29	1.29
		$x = 1.5$ cm,	u (μm)	5.29	5.46	5.41	5.42	5.41	5.42	5.42	5.42
		$y = 20$ μm	v (mm)	1.29	1.29	1.29	1.29	1.29	1.29	1.29	1.29

adjustment.

For the purpose of predicting the vertical displacements at the bottom surface of LCEs system which is induced by a specific mechanical load in temperature field, the coefficients a_n of the mechanical load in the database are the input information while the vertical displacements of the corresponding position are the output information, as shown in the Fig. 2(a). On the other hand, for the purpose of inversing the mechanical load which induces a specific elastic deformation of the LCEs system in temperature field, the vertical displacements at the corresponding position in the database are the input information while the coefficients a_n of the mechanical load in the database are the output information, as shown in the Fig. 2(b).

3. Results and discussion

3.1. Convergence and comparison studies

An LCEs system consists of two side LCE layers and a flexible substrate layer in middle as shown in Fig. 3 is considered in the following convergence and comparison studies to verify the accuracy and correctness of the present analytical model. The length of the structure is $L = 2$ cm. The thickness of each layer is $h_1 = h_2 = h_3 = 10$ μm, the Young's modulus are $E_1 = E_3 = 6$ MPa, $E_2 = 4 \times 10^3$ MPa, and the Poisson ratio are $\mu_1 = \mu_3 = 0.499$, $\mu_2 = 0.34$. The coefficients of thermal expansion are $\alpha_1 = \alpha_3 = -1.5 \times 10^{-4}$ °C $^{-1}$, and $\alpha_2 = 2.5 \times 10^{-5}$ °C $^{-1}$. The thermal conductivities are $k_1 = k_3 = 0.22$ W/(m·°C), $k_2 = 0.12$ W/(m·°C). Two mechanical loads are considered in the example by uniform, and quadratic polynomial distribution functions, respectively. The bottom and top surfaces of LCEs system are subjected to a constant temperature load $T_b(x) = 36$ °C and $T_t(x) = 37$ °C, respectively.

Table 1 shows the convergence of the displacements at two points, where the coordinates (x, y) equal to (0.5 cm, 10 μm) and (1.5 cm, 20 μm), under two different mechanical loads at the bottom surface of laminated LCEs beam. It can be seen from Table 1 that the values of displacements converge with the increase of expansion order m. The results of $m = 40$ is the same as those of $m = 30$ and 35. Therefore, in the following numerical examples, the series terms are all set to $m = 40$.

In the finite element model (FEM) model, two-dimensional four-node plane stress PLANE13 element is selected for finite element analysis. The material parameters of three beams mentioned above are input into the Material Models function of the software, and then assigned to different beams before meshing. The displacement constraints corresponding to a simply supported beam are applied in the finite element software. Temperature condition 37 °C is added to the line at the top and 36 °C is added to the line at the bottom of the model. The mesh density analysis is presented in Table 2 to ensure the convergence and reliability of the FE results. It can be seen from Table 2 that the results converge with the increase of the number of elements. Table 3 shows the comparison of the displacements results between the present analytical model and the FE model with 24000 elements. Since the LCEs systems under the thermo-mechanical loads possess the symmetries, six points at the bottom surface on the left side of the laminated beam are considered with the x coordinates equal to 0 cm, 0.2 cm, 0.4 cm, 0.6 cm, 0.8 cm, and 1 cm, respectively.

Eq. (25) is used to evaluate the relative error between the analytical results from the present model and numerical results from FEM. It can be seen from Table 3 that the relative errors between the present analytical model and FEM is less than 2.5%.

$$E = \left| \frac{F - R}{F} \right| \times 100\% \tag{25}$$

Where F is the FEM results, R is the present analytical results.

3.2. Parametric studies

The following numerical examples are presented to study the influence of thermo-mechanical load and layer thickness on the vertical displacements at the bottom surface of the LCEs system. Unless otherwise mentioned, calculation parameters of the LCEs system used in the following examples are the same as those mentioned in Section 3.1.

Fig. 4 shows the influence of temperature on the vertical displacement at the bottom surface of the LCEs system which subjected to uniform and quadratic polynomial distributed loads at the bottom surface respectively. The LCEs system is pasted on the surface of the heart, and the temperature cannot be kept constant all the time. When a fever occurs, the body temperature may rise from 36 °C to 40 °C. The temperature at bottom surface of the system is kept constant at 36 °C. The top surface of the system is considered with different temperature loads from 36 °C to 40 °C with a gradient of 1 °C. It can be seen from Fig. 4 that the bottom surface become contraction with the increase of the

Table 2
Result of mesh density analysis.

Position	Dis.	Element quantities (Element size)					
		6000 (5μm × 20μm)	12000 (5μm × 10μm)	15000 (2μm × 20μm)	24000 (5μm × 5μm)	30000 (2μm × 10μm)	60000 (2μm × 5μm)
$x = 0.1$ cm,	u (μm)	−15.69	−11.55	−7.89	−7.88	−7.88	−7.88
$y = 0$ μm	v (mm)	0.0091	0.0091	0.0091	0.0091	0.0091	0.0091
$x = 0.8$ cm,	u (μm)	−9.58	−5.43	1.77	−1.76	−1.76	−1.76
$y = 20$ μm	v (mm)	0.045	0.045	0.045	0.045	0.045	0.045

Table 3
Comparison of the present displacements with FEM results at bottom surface under different mechanical loads.

$q(x)$ (N/cm)	Dis	Method	$x = 0$ cm	$x = 0.2$ cm	$x = 0.4$ cm	$x = 0.6$ cm	$x = 0.8$ cm	$x = 1$ cm
0.1	u (μm)	Present	−7.254	−5.670	−4.131	−2.697	−1.331	0
		FE	−7.224	−5.637	−4.098	−2.663	−1.298	0
		Error	***0.41%***	***0.58%***	***0.80%***	***1.26%***	***2.48%***	***0%***
	v (mm)	Present	0	0.2060	0.3877	0.5290	0.6184	0.6490
		FE	0	0.2045	0.3848	0.5247	0.6126	0.6417
		Error	***0%***	***0.73%***	***0.75%***	***0.81%***	***0.94%***	***1.13%***
$(x\text{-}1)^2+0.1$	u (μm)	Present	−4.366	−3.019	−2.022	−1.260	−0.609	0
		FE	−4.353	−3.003	−2.005	−1.244	−0.594	0
		Error	***0.30%***	***0.53%***	***0.84%***	***1.27%***	***2.46%***	***0%***
	v (mm)	Present	0	0.5799	1.081	1.460	1.693	1.772
		FE	0	0.5762	1.074	1.449	1.678	1.753
		Error	***0%***	***0.64%***	***0.65%***	***0.75%***	***0.89%***	***1.07%***

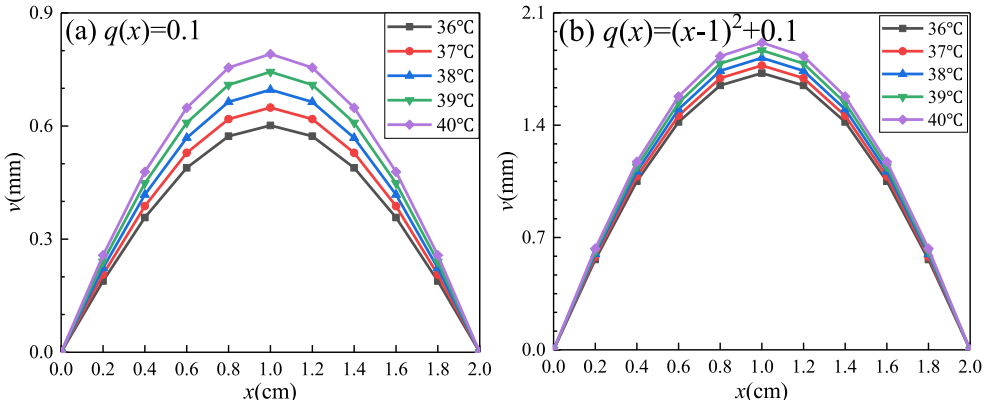

Fig. 4. The influence of temperature on the vertical displacement at the bottom surface of LCEs system.

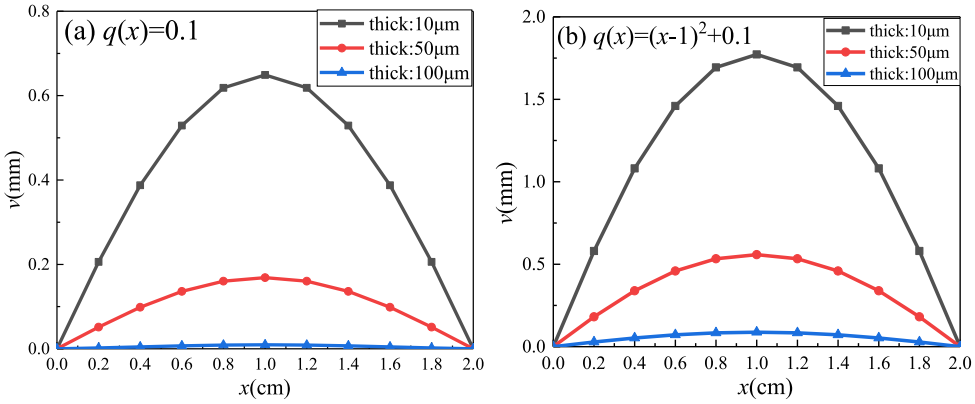

Fig. 5. The influence of LCE thickness on the vertical displacement at the bottom surface of LCEs system.

Table 4
Calculation parameters used for establishing the database of a LCEs system in a temperature field (T_b (x) = 36 °C, T_t (x) = 37 °C)

Coordinates of six points at left half of the bottom surface	Coefficients	Scale of coefficients
$x = 0$ to 1 cm with a gradient of 0.2 cm; $y = 0$	a_2	From 0 to 5 a gradient of 0.1
	a_1	From 0 to 1 a gradient of 0.1

temperature. This is because LCE has a negative thermal expansion. The numerical results show that the vertical displacement at the middle of the laminated LCEs system increase 0.047mm with each additional 1 °C of temperature increase. It is indicated that the deformation of laminated LCEs system due to temperature variation is limited within the range of human temperature changes from 36 °C to 40 °C.

Fig. 5 shows the influence of thickness of each LCE layer on the vertical displacement of the LCEs system. The thickness of the flexible substrate in the middle layer is kept as 10 μm, and the thickness of each LCE layer are 10 μm, 50 μm and 100 μm respectively. It can be seen from Fig. 5 that the thickness of each LCE layer has a significant influence on

Table 5
Five group of mechanical loads applied on the bottom surface of the LCEs system in a temperature field and their corresponding vertical displacements.

No.	The given coefficients of mechanical load		The given vertical displacements at the bottom surface ($y = 0$) of LCEs system obtained by present analytical solution (mm)					
	a_1	a_2	Point 1 ($x = 0$ cm)	Point 2 ($x = 0.2$ cm)	Point 3 ($x = 0.4$ cm)	Point 4 ($x = 0.6$ cm)	Point 5 ($x = 0.8$ cm)	Point 6 ($x = 1.0$ cm)
#1	0.65	0	0	1.245	2.353	3.219	3.769	3.957
#2	0.2	0.135	0	0.445	0.839	1.144	1.336	1.402
#3	0.8	0.05	0	1.547	2.923	3.999	4.682	4.916
#4	0.6	1.563	0	1.735	3.258	4.429	5.163	5.412
#5	1	0.86	0	2.227	4.199	5.732	6.698	7.029

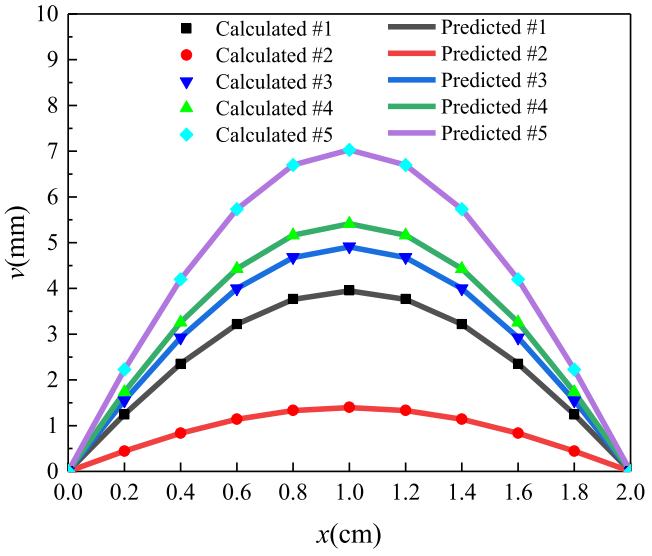

Fig. 6. Comparison between the predicted solutions and the analytical solutions of vertical displacements.

the vertical displacement at the bottom surface of LCEs system. The displacement at the middle of the bottom surface of the LCEs system with the thickness of each LCE layer of 50 μm is reduced by more than 65% compared with that of the system with 10 μm LCE layers. The displacement of the system with the thickness of each LCE layer of 100 μm is reduced by more than 98% compared with that of the system with 10 μm LCE layers. Therefore, reducing the thickness of LCE layer is an effective way to improve the deformation performance of the LCEs system.

3.3. Verification of BP neural network prediction

The BP neural network model introduced in this paper can be used to predict the deformation of the LCEs system subjected the mechanical surface load, as well as inverse mechanical load which induces the specific deformation in a temperature field. A database with 561 sets of data consists of both the coefficients of mechanical load in Eq. (23) and corresponding displacements of six points at left half of bottom surface of the LCEs system in the temperature field $T_b(x) = 36$ °C, $T_t(x) = 37$ °C is obtained by the present analytical solution. The database is used to train the BP neural network model. The scales of the mechanical load coefficients used for training the BP model is presented in Table 4. There are five new data sets presented in Table 5, which are not part of the training data, used to evaluate the accuracy of the BP neural network to predict the mechanical solution of the LCEs system. The adjustment constant J is selected as 6 in this example. So the hidden layer of the BP neural network is set as 9 based on the in Eq. (23). The learning rate, the maximum number of network training and the minimum mean square error are set as 0.01, 1000 and 0.00001 respectively.

3.3.1. Predict the deformation subjected to mechanical load

In this section, the coefficients a_n are set as the input information and the vertical displacements at the bottom surface are set as the output information to establish the BP model. The predicted displacements are compared with the calculated results from the present analytical solutions. The prediction error is calculated by Eq. (25) to represent the accuracy of the neural network.

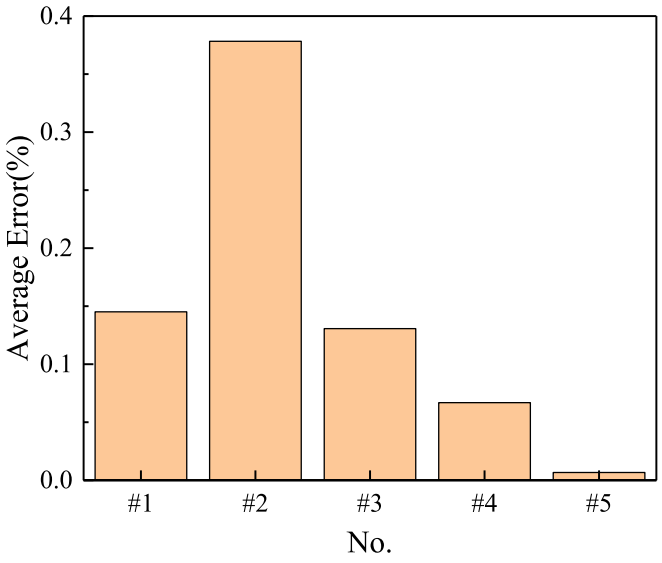

Fig. 7. Prediction errors of the vertical displacements.

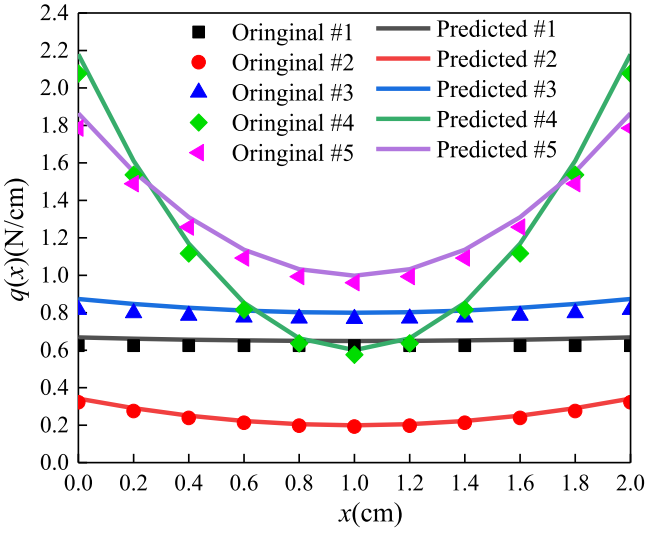

Fig. 8. Comparison between the predicted solutions and the analytical solutions of mechanical loads.

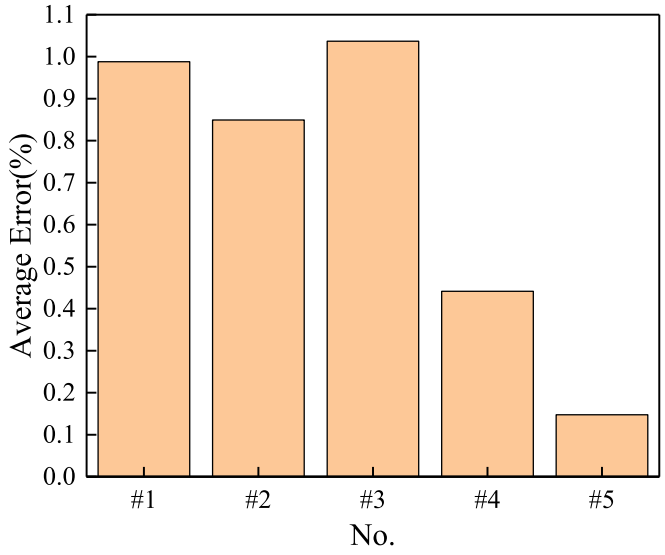

Fig. 9. Prediction errors of mechanical loads.

$$error = \left|\frac{R-P}{R}\right| \times 100\% \tag{26}$$

Where P is the predicted results, R is the calculated analytical results. Five sets of coefficients of mechanical loads listed in Table 5 are used for the prediction. Fig. 6 shows the comparison between the given vertical displacements by presented analytical solutions and the predicated solutions by BP model. It can be seen from Fig. 6 that the predicted results are in good agreement with the calculated displacements. The error analysis of vertical displacements predicted by BP neural network is shown in Fig. 7. It can be seen from Fig. 7 that the average error of displacement prediction by BP neural network is less than 0.4%. It is indicated from Fig.7 that BP neural network is an effective method to predict vertical displacement of a LCEs system in a temperature field subjected to continuously distributed mechanical loads. And the results shows that the size of the database used in this paper is enough to predict the results with low error.

3.3.2. *Inverse mechanical load based on the deformation*

In this section, the vertical displacements are selected as the input information and the coefficients a_n of the mechanical load are selected as the output information to establish the BP model. Five sets of displacements at six points at the left half of bottom surface of the laminated beam listed in Table 5 are used for inversing the coefficients of mechanical load in Eq. (23). Fig. 8 shows the comparison between the curves of inversed mechanical loads and those of given mechanical loads. It can be seen from Fig. 8 that the inversed mechanical loads agree with the curves of given mechanical loads. The error analysis of mechanical loads inversed by BP neural network is shown in Fig. 9. It can be seen from Fig. 9 the average errors of mechanical load predicted by BP neural network are less than 1.1%. It confirms the effectiveness of using BP neural network to inverse the mechanical load which induces the vertical displacement at the bottom surface of a LCEs system in a specific temperature field.

4. Concluding remarks

This paper presents a convenient and efficient method to predict the mechanical solutions of a laminated LCEs system subjected to combined thermo-mechanical load based on an analytical model and a BP neural network. The analytical solution of a simply supported laminated beam is derived by heat conduction and thermoelastic theory and verified by the convergence and comparison studies. The relative error between the analytical solution and the FEM results is less than 2.5%. The BP neural network models are established by training a database which contains the information of 561 sets of mechanical solutions obtained by the present analytical solutions. Some numerical examples are presented to analyse the influence of thermo-mechanical load and the thickness of LCE on the mechanical properties of the LCEs system. Two BP neural network models are presented to show the accuracy of the predictions. Following conclusions are presented based on the results of numerical examples:

(1) Within the body temperature changes from 36 °C to 40 °C, the deformation of LCE laminated system is limited. If greater deformation is required, a mechanical load needs to be applied.
(2) Reducing the thickness of LCE layer is an effective way to improve the deformation of the LCEs system. It is necessary to select LCE layer with small thickness to meet the deformation requirements of the heart.
(3) BP neural network is an efficient method to predict the mechanical solutions of a laminated LCEs system subjected to a thermo-mechanical load through database learning. The accuracy of vertical displacement at the bottom surface of LCEs system predicted by BP neural network can reach 99.6%, while the accuracy of mechanical load applied at the bottom surface of LCEs system inversed by BP neural network can reach 98.9%.

CRediT authorship contribution statement

Thebano Santos: Writing – review & editing.

Declaration of competing interest

The authors declare that they have no known competing financial interests or personal relationships that could have appeared to influence the work reported in this paper.

Acknowledgement

The financial supports from the National Natural Science Foundation of China (51805147, 52178474), Fundamental Research Funds for the Central Universities (B210202127) and Changzhou Sci&Tech Program (CJ20210138) are greatly acknowledged.

Appendix

The elements in the matrix $\boldsymbol{TF}_{mi}$ are as follows:

$$TF_{mi}^{11} = \cosh(\alpha_m y_i)$$

$$TF_{mi}^{12} = \sinh(\alpha_m y_i)$$

$$TF_{mi}^{13} = \frac{3-\mu_i}{1+\mu_i}\frac{L}{m\pi}\sinh(\alpha_m y_i) + y_i \cosh(\alpha_m y_i)$$

$$TF_{mi}^{14}=\frac{3-\mu_i}{1+\mu_i}\frac{L}{m\pi}\cosh(\alpha_m y_i)+y_i\sinh(\alpha_m y_i)$$

$$TF_{mi}^{21}=\sinh(\alpha_m y_i)$$

$$TF_{mi}^{22}=\cosh(\alpha_m y_i)$$

$$TF_{mi}^{23}=y_i\sinh(\alpha_m y_i)$$

$$TF_{mi}^{24}=y_i\cosh(\alpha_m y_i)$$

$$TF_{mi}^{31}=\alpha_m\cosh(\alpha_m y_i)\frac{-E_i}{1+\mu_i}$$

$$TF_{mi}^{32}=\alpha_m\sinh(\alpha_m y_i)\frac{-E_i}{1+\mu_i}$$

$$TF_{mi}^{33}=\left[\frac{3+\mu_i}{1+\mu_i}\sinh(\alpha_m y_i)+\alpha_m y_i\cosh(\alpha_m y_i)\right]\frac{-E_i}{1+\mu_i}$$

$$TF_{mi}^{34}=\left[\frac{3+\mu_i}{1+\mu_i}\cosh(\alpha_m y_i)+\alpha_m y_i\sinh(\alpha_m y_i)\right]\frac{-E_i}{1+\mu_i}$$

$$TF_{mi}^{41}=\alpha_m\cosh(\alpha_m y_i)\frac{E_i}{1+\mu_i}$$

$$TF_{mi}^{42}=\alpha_m\sinh(\alpha_m y_i)\frac{E_i}{1+\mu_i}$$

$$TF_{mi}^{43}=\left[\frac{1-\mu_i}{1+\mu_i}\sinh(\alpha_m y_i)+\alpha_m y_i\cosh(\alpha_m y_i)\right]\frac{E_i}{1+\mu_i}$$

$$TF_{mi}^{44}=\left[\frac{1-\mu_i}{1+\mu_i}\cosh(\alpha_m y_i)+\alpha_m y_i\sinh(\alpha_m y_i)\right]\frac{E_i}{1+\mu_i}$$

$$TF_{mi}^{51}=\alpha_m\sinh(\alpha_m y_i)\frac{E_i}{1+\mu_i}$$

$$TF_{mi}^{52}=\alpha_m\cosh(\alpha_m y_i)\frac{E_i}{1+\mu_i}$$

$$TF_{mi}^{53}=\left[\frac{2}{1+\mu_i}\cosh(\alpha_m y_i)+\alpha_m y_i\sinh(\alpha_m y_i)\right]\frac{E_i}{1+\mu_i}$$

$$TF_{mi}^{54}=\left[\frac{2}{1+\mu_i}\sinh(\alpha_m y_i)+\alpha_m y_i\cosh(\alpha_m y_i)\right]\frac{E_i}{1+\mu_i}$$

The elements in the matrix $\boldsymbol{TT}_{mi}$ are as follows:

$$TT_{mi}^{11}=-2\alpha_i\frac{L}{m\pi}\cosh(\alpha_m y_i)$$

$$TT_{mi}^{12}=-2\alpha_i\frac{L}{m\pi}\sinh(\alpha_m y_i)$$

$$TT_{mi}^{21}=0$$

$$TT_{mi}^{22}=0$$

$$TT_{mi}^{31}=\alpha_i\cosh(\alpha_m y_i)\frac{E_i}{1+\mu_i}$$

$$TT_{mi}^{32}=\alpha_i\sinh(\alpha_m y_i)\frac{E_i}{1+\mu_i}$$

$$TT_{mi}^{41}=-\alpha_i\cosh(\alpha_m y_i)\frac{E_i}{1+\mu_i}$$

$$TT_{mi}^{42}=-\alpha_i\sinh(\alpha_m y_i)\frac{E_i}{1+\mu_i}$$

$$TT_{mi}^{51} = -\alpha_i \cosh(\alpha_m y_i) \frac{E_i}{1+\mu_i}$$

$$TT_{mi}^{52} = -\alpha_i \sinh(\alpha_m y_i) \frac{E_i}{1+\mu_i}$$

References

Asadi, H., Kiani, Y., Shakeri, M., Eslami, M.R., 2014. Exact solution for nonlinear thermal stability of hybrid laminated composite Timoshenko beams reinforced with SMA fibers. Compos. Struct. 108, 811–822.

Bagheripoor, M., Bisadi, H., 2013. Application of artificial neural networks for the prediction of roll force and roll torque in hot strip rolling process. Appl. Math. Model. 37, 4593–4607.

Balla, K., Sevilla, R., Hassan, O., et al., 2021. An application of neural networks to the prediction of aerodynamic coefficients of aerofoils and wings. Appl. Math. Model. 10, 456–479.

Blanc, M., Touratier, M., 2007. An efficient and simple refined model for temperature analysis in thin laminated composites. Compos. Struct. 77, 193–205.

Carrera, E., 2001. Developments, ideas, and evaluations based upon Reissner's mixed variational theorem in the modelling of multilayered plates and shells. Appl. Mech. Rev. 54, 301–329.

Carrera, E., Giunta, G., 2010. Refined beam theories based on a unified formulation. Int. J. Appl. Mech. 2, 117–143, 01.

Carrera, Erasmo, Fazzolari, Fiorenzo A., Cinefra, Maria, 2016a. Thermal Stress Analysis of Composite Beams, Plates and Shells: Computational Modelling and Applications. Academic Press.

Carrera, E., Entezari, A., Filippi, M., Kouchakzadeh, M.A., 2016b. 3D thermoelastic analysis of rotating disks having arbitrary prole based on A variable kinematic 1D finite element method. J. Therm. Stresses 39, 1–16.

Do, D., Nguyen-Xuan, H., Lee, J., 2020. Material optimization of tri-directional functionally graded plates by using deep neural network and isogeometric multimesh design approach. Appl. Math. Model. 87, 501–533.

Eslami, M.R., Hetnarski, R.B., Ignaczak, J., Noda, N., Sumi, N., Tanigawa, Y., 2013. Theory of Elasticity and Thermal Stresses. Springer, Dordrecht.

Gennes, P.D., 1997. Un muscle artificiel semi-rapide. Comptes Rendus Acad. Sci. - Ser. IIB Mech. Phys., Chem., Astron. 324, 343–348.

Gennes, P.D., Hébert, M., Kant, R., 1997. Artificial muscles based on nematic gels. Macromol. Symp. 113, 39–49.

Giunta, Gaetano, et al., 2013. A thermo-mechanical analysis of functionally graded beams via hierarchical modelling. Compos. Struct. 95, 676–690.

Hagan, M.T., Demuth, H.B., Beale, M.H., 2002. Neural Network Design. China Machine Press.

Kapuria, S., Dumir, P.C., Ahmed, A., 2003. An efficient higher order zigzag theory for composite and sandwich beams subjected to thermal loading. Int. J. Solid Struct. 40, 6613–6631.

Li, M.H., Keller, P., Yang, J., et al., 2004. An artificial muscle with lamellar structure based on a nematic triblock copolymer. Adv. Mater. 16, 1922–1925.

Liu, R., Tang, F., Wang, Y., et al., 2021. A modified NK algorithm based on BP neural network and DEMATEL for evolution path optimization of urban innovation ecosystem. Complex & Intelligent Systems 20.

Lu, H.F., Wang, M., Chen, X.M., et al., 2019. Interpenetrating liquid crystal polyurethane/polyacrylate elastomer with ultrastrong mechanical property. J. Am. Chem. Soc. 141, 14364–14369.

Mitchell, T.M., 2003. Machine Learning. McGraw-Hill.

Pidaparti, R., Palakal, M.J., 2015. Material model for composites using neural networks. AIAA J. 31, 1533–1535.

Qian, H., Zhou, D., Liu, W.Q., et al., 2015a. Elasticity Solution of Laminated Beams Subjected to thermo-loads[J], vol. 6. Journal of Central South University, pp. 2297–2305.

Qian, H., Zhou, D., Liu, W.Q., et al., 2015b. Elasticity solution of laminated beams subjected to thermo-loads. J. Cent. S. Univ. 22, 2297–2305.

Ren, Z., Yuan, J., Su, X., et al., 2021. Thermo-mechanical modeling and experimental validation for multilayered metallic microstructures. Microsyst. Technol. 27, 2579–2587.

Sattari, M.T., Yurekli, K., Pal, M., 2013. Performance evaluation of artificial neural network approaches in forecasting reservoir inflow. Appl. Math. Model. 36, 2649–2657.

Sharma, J.N., Kaur, R., 2015. Flexural response of thermoelastic thin beam resonators due to thermal and mechanical loads. Int. J. Mech. 101–102, 170–179.

Shenoy, D.K., Iii, D., Srinivasan, A., et al., 2002. Carbon coated liquid crystal elastomer film for artificial muscle applications. Sensors & Actuators A Physical 96, 184–188.

Teti, R., Caprino, G., 1994. Prediction of composite laminate residual strength based on a neural network approach. Appl. Artif. Intell. Eng. IX, 6.

Thai, H.T., Vo, T.P., 2012. Bending and free vibration of functionally graded beams using various higher-order shear deformation beam theories. Int. J. Mech. Sci. 62, 57–66.

Thomsen, D.L., Keller, P., Naciri, J., et al., 2001. Liquid crystal elastomers with mechanical properties of a muscle. Macromolecules 34, 5868–5875.

Timoshenko, S., 1925. Analysis of bimetal thermostats, 1917-1983 J. Opt. Soc. Am. 11, 233–255.

Wu, Z., Zhao, Y., 2012. Enhanced Reddy's beam theory and thermal stress analysis. Fuhe Cailiao Xuebao/Acta Materiae Compositae Sinica 29, 246–250.

Xu, Y.P., Zhou, D., 2009. Elasticity solution of multi-span beams with variable thickness under static loads. Appl. Math. Model. 33, 2951–2966.

Xu, Y.P., Zhou, D., 2012. Two-dimensional thermoelastic analysis of beams with variable thickness subjected to thermo-mechanical loads. Appl. Math. Model. 36, 5818–5829.

Zhang, Z., Zhou, D., Fang, H., Zhang, J., Li, X., 2019. Analysis of laminated beams with temperature-dependent material properties subjected to thermal and mechanical loads. Compos. Struct. 227, 111304.

Ziane, K., Zebirate, S., Zaitri, A., 2015. Predicting the Fatigue Strength of Different Composite Laminates of Wind Turbine Blades. Third Euro-Mediterranean Meeting on Functionalized Materials EMM-FM, 2015.